Climate pathways behind phytoplankton-induced atmospheric warming

Rémy Asselot [1,*], Frank Lunkeit [2], Philip Holden [3], and Inga Hense [1]

[1]Institute for Marine Ecosystem and Fishery Science, Center for Earth System Research and Sustainability, University of Hamburg, Hamburg, Germany
[2]Meteorological Institute, Center for Earth System Research and Sustainability, University of Hamburg, Hamburg, Germany
[3]Environment, Earth and Ecosystems, The Open University, Walton Hall, Milton Keynes, MK7 6AA, UK
[*]Now at Ifremer, University of Brest, CNRS, IRD, Laboratoire d'Océanographie Physique et Spatiale (LOPS), UMR6523, Centre de Bretagne, 29280 Plouzané, France

Correspondence: Rémy Asselot (remy.asselot@ifremer.fr)

Abstract. We investigate in which ways marine biologically-mediated heating increases the surface atmospheric temperature. While the effects of phytoplankton light absorption on the ocean have gained attention over the past years, the impact of this biogeophysical mechanism on the atmosphere is still unclear. Phytoplankton light absorption warms the surface of the ocean which in turn affects the air-sea heat and CO_2 exchanges. However, the contribution of air-sea heat versus CO_2 fluxes in the phytoplankton-induced atmospheric warming has not been yet determined. Different so-called climate pathways are involved. We distinguish heat exchange, CO_2 exchange, dissolved CO_2, solubility of CO_2 and sea-ice covered area. To shed light, we employ the EcoGEnIE Earth system model that includes a new light penetration scheme and isolate the effects of individual fluxes. Our results indicate that phytoplankton-induced changes in air-sea CO_2 exchange warm the atmosphere by 0.71°C due to higher greenhouse gas concentrations. The phytoplankton-induced changes in air-sea heat exchange cool the atmosphere by 0.02°C due to a larger outgoing longwave radiation. Overall, the enhanced air-sea CO_2 exchange due to phytoplankton light absorption is the main driver in the biologically-induced atmospheric heating.

1 Introduction

Previous studies have shown that marine biota can modify the light penetration in the ocean with consequences on the atmospheric temperature and on the climate system (Shell et al., 2003; Wetzel et al., 2006; Gnanadesikan and Anderson, 2009). Using an Earth system model (ESM) of intermediate complexity, we identify and compare the climate pathways behind the changes in atmospheric temperature due to phytoplankton light absorption.

Marine biota and phytoplankton play a major role in the absorption of light and therefore in the vertical distribution of heat in the upper layers of the ocean (Kowalczuk et al., 2019). Indeed, observational evidence supports the hypothesis that chlorophyll increases the upper ocean heat uptake. For instance, satellite observations show that phytoplankton blooms can cause an increase of sea surface temperature (SST) of 1.5°C (Kahru et al., 1993). Furthermore, previous remote sensing data indicate

an increase in local SST of 4.5°C on a 4 day-timescale due to the presence of phytoplankton blooms (Capone et al., 1998). Recent high-resolution in situ observations in the Indo-West Pacific Ocean highlight large anomalies of temperature of 0.95°C in the uppermost skin layer of the ocean when large phytoplankton blooms appear (Wurl et al., 2018). However, all these ob-
25   servations are either on a short time scale or in a geographically limited area. To study the larger-scale impact of phytoplankton light absorption and its relative magnitude, Earth system models are employed.

Models of differing complexity are used to study the effect of phytoplankton light absorption. For instance, using ocean-only (Anderson et al., 2007) or general circulation models, several studies focusing on the tropical Pacific Ocean (Murtugudde
30   et al., 2002; Lengaigne et al., 2007; Löptien et al., 2009) or on the Arctic Ocean (Lengaigne et al., 2009) report an increase of SST between 0.5-2°C due to phytoplankton light absorption. A warming of the ocean surface induced by marine biota has consequences on the overall climate system. For instance, Patara et al. (2012) find that an increase of SST due to phytoplankton light absorption increases the atmospheric humidity content thereby increasing the greenhouse effect and the atmospheric temperature locally by up to 0.5°C. Furthermore, phytoplankton can amplify locally the seasonal temperature of the lowest
35   atmospheric layer by 1°C, changing the Walker and Hadley circulation (Shell et al., 2003).

It is therefore known that phytoplankton light absorption has a non-negligible role on the atmospheric temperature but which climate pathway is the most important behind this warming is still unclear. Phytoplankton light absorption affects the surface atmospheric temperature via two climate pathways. First, various modeling studies suggest that biologically-induced surface
40   water heating can increase the air-sea heat exchange (Capone et al., 1998; Oschlies, 2004; Wetzel et al., 2006) with consequences on the formation of tropical storms and monsoons in the Arabian Sea (Sathyendranath et al., 1991). Second, the solubility of gases and thus also the air-sea CO_2 exchange is affected by phytoplankton light absorption. For instance, Manizza et al. (2008) study the impact of this biogeophysical mechanism on the air-sea flux of CO_2 and find that phytoplankton light absorption has a small outgassing effect on a global scale with high regional fluctuations.

45

However, none of these studies have analyzed, disentangled and compared the changes in both air-sea heat and CO_2 exchange due to phytoplankton light absorption. To shed light on the biologically-induced atmospheric warming, we use a recent Earth system model called EcoGEnIE (Ward et al., 2018). In an earlier study, we implemented phytoplankton light absorption in this model (Asselot et al., 2021). We consider two different biologically-induced changes: changes in air-sea heat and
50   changes in air-sea CO_2 exchange (Figure 1). The air-sea CO_2 exchange can be influenced by the dissolved oceanic CO_2 in three different ways: through 1) changes in the biogeochemical pumps as a result of phytoplankton light absorption. For instance, Manizza et al. (2008) have shown that changes in oceanic circulation due to phytoplankton light absorption enhance the vertical supply of nutrients, increasing the relative abundance of calcifiers. As a consequence, the primary production and the export production of organic matter increase. Through 2) decrease in CO_2 solubility due to higher SST, increasing the
55   atmospheric CO_2 concentrations and the greenhouse gas effect. Through 3) decrease in sea-ice formation because sea-ice acts

as an ocean cap that blocks gas exchanges. To achieve the disentangling of the specific climate pathways, we turn them on and off by prescribing values in our ESM in order to isolate their impact on the climate system.

2 Model description

Our motivation is to study the interactions between the marine ecosystem, the biogeochemistry, the biogeophysics and the climate system. These interactions are computationally expensive in high-resolution models therefore we used an Earth system model of intermediate complexity (Claussen et al., 2002). The Earth system model employed is the carbon-centric Grid-Enabled Integrated Earth system model (cGEnIE) (Lenton et al., 2007) composed of several modules describing the dynamics of the Earth system (Figure 2). This model has been previously calibrated and compared to observations (Edwards and Marsh, 2005; Lenton et al., 2006; Ridgwell et al., 2007; Marsh et al., 2011). Moreover, this model is widely used to study past climate and changes in the carbon cycle over geological times (Ödalen et al., 2018; Greene et al., 2019; Adloff et al., 2020), past mass extinctions (Alvarez et al., 2019) and biogeochemistry processes (Meyer et al., 2016). Additionally, cGEnIE has been employed to assess the sensitivity of atmospheric CO_2 to biogeochemical pumps, ocean circulation and climate feedbacks in the Southern Ocean (Cameron et al., 2005). A new ecosystem component (ECOGEM) is associated with cGEnIE to form the recent EcoGEnIE model (Ward et al., 2018). EcoGEnIE is used to determine the link between the marine plankton ecosystem and various past climate scenarios (Wilson et al., 2018) with focus on phosphorus inventory (Reinhard et al., 2020). For our study, the model combines different components including ocean hydrodynamics, atmosphere, sea-ice, ocean biogeochemistry and marine ecosystem component. We do not consider a terrestrial component meaning that the land surface is essentially passive. We use the same configuration as described in detail by Asselot et al. (2021) and the following description only refers to our specific model setup.

2.1 Modules

2.1.1 The physical components

The physics of the model contains a frictional-geostrophic ocean circulation (GOLDSTEIN), coupled to a 2D energy-moisture balance model of the atmosphere (EMBM) and a thermodynamic sea-ice model (GOLDSTEINSEAICE) (Edwards and Marsh, 2005; Marsh et al., 2011). Heat and moisture are exchanged between the three components and act as a coupling strategy. The oceanic component calculates the horizontal and vertical redistribution of heat, salinity and biogeochemical elements via advection, convection and mixing. The ocean module is configured on a 36×36 horizontal grid. The horizontal grid is uniform in longitude and uniform in sine latitude, giving $\sim 3.2°$ latitudinal increments at the equator increasing to $19.2°$ in the highest latitude. This horizontal grid has been used for previous biogeochemical simulations (Cameron et al., 2005; Colbourn, 2011). We consider 32 vertical oceanic layers increasing logarithmically from 29.38 m for the surface layer to 456.56 m for the deepest layer. This vertical resolution is already used to study the relative importance of biogeophysical and biogeochemical mechanisms on the climate system (Asselot et al., 2021).

The atmospheric component is based closely on the UVic Earth system model (Weaver et al., 2001). The prognostic variables are atmospheric temperature and specific humidity. Precipitation removes instantaneously all moisture corresponding to an excess above a relative humidity threshold. The wind stress is prescribed and identical between all simulations, the temperature cannot affect the wind stress.

The sea-ice component solves the equation for part of the ocean covered by sea-ice. The prognostic variables are ice thickness and ice areal fraction. The transport of sea-ice includes sources and sinks of these variables. The growth or decay of sea ice depends on the net heat flux into the ice. The dynamics in this module consist of advection by currents and diffusion. Sea-ice doesn't limit the penetration of photosynthetically available radiation in the ocean.

2.1.2 Ocean biogeochemistry component

The biogeochemical module (BIOGEM) represents the transformation and spatial redistribution of biogeochemical tracers (Ridgwell et al., 2007). The state variables are inorganic and organic matter. The biological uptake is represented by an implicit biological community: nutrients are directly converted into organic matter via an uptake rate. The biological uptake is limited by light, temperature and nutrient availability. Organic matter is partitioned into dissolved and particulate phases (DOM and POM). For this study, BIOGEM does not consider a temperature dependency on iron solubility and iron bioavailability. Our model setup includes iron (Fe) and phosphate (PO_4) as limiting nutrients. Similar to Asselot et al. (2021), we do not consider nitrate here. Moreover, the surface production is redistributed in the water column as a depth-dependent flux. To achieve this, the surface export is divided between refractory organic matter remineralised close to the seafloor and labile organic matter mostly remineralised in the upper water column (Ridgwell et al., 2007). Furthermore, because we do not consider a sediment component, all organic matter reaching the sea-floor is instantaneously remineralised. Calcium carbonate ($CaCO_3$) is represented in the model and its dissolution below the surface follows the same profile as the remineralisation of POM. Additionally, $CaCO_3$ production is parameterised as a fixed ratio to POC production, and so is not independent in our model setup. Recent studies have implemented and calibrated a temperature-dependent remineralization in the the model (Crichton et al., 2021; Armstrong McKay et al., 2021) but this parameterization is not included in our model setup. Furthermore, BIOGEM calculates the air-sea CO_2 and O_2 exchange. The value of atmospheric CO_2 predicted by BIOGEM is used as input for the radiative scheme of the atmospheric component, thus providing climate feedback.

2.1.3 Ecosystem component

The marine ecosystem component (ECOGEM) represents the marine plankton community and associated interactions within the ecosystem (Ward et al., 2018). The biological uptake in ECOGEM replaces the BIOGEM uptake calculation and is limited by light, temperature and nutrient availability. Plankton biomass and organic matter are subject to processes such as resource competition and grazing before being passed to DOM and POM. Several ecophysiological parameters are size-dependent such as: maximum nutrient uptake rate, cell carbon quotas, grazing and partitioning between DOM and POM. Additionally, the nutrient uptake, photosynthesis and predation are temperature-dependent. The ecosystem is divided into different plankton functional types (PFTs) with specific traits. Each PFT is sub-divided into size classes with specific size-dependent traits. Here,

120 we consider only two PFTs: phytoplankton and zooplankton (Appendix A1). Phytoplankton is characterized by nutrient uptake and photosynthesis whereas zooplankton is characterized by predation traits. Zooplankton grazing depends on the concentration of prey biomass, with predominantly grazing on prey that are 10 times smaller than themselves. Each population is associated with biomass state variables for carbon, phosphate, iron and chlorophyll. The production of dead organic matter is a function of mortality and messy feeding, with partitioning between non-sinking dissolved and sinking particulate organic matter. Finally,

125 plankton mortality is reduced at very low biomass such that plankton cannot become extinct.

2.2 Light absorption in the ocean

In the previous model version (Ward et al., 2018), light was only absorbed by phytoplankton. In the model version of Asselot et al. (2021), a new light scheme is implemented where the absorbed light by phytoplankton is converted into heat and is able to affect the oceanic temperature. Furthermore, light absorption takes place throughout the water column and is not restricted to

130 the first oceanic layer anymore. The light absorption scheme is a coupling between Eq. 1 and Eq. 2. For simplicity, in our model configuration, the incoming shortwave radiation does not vary seasonally. We look at long-term changes in the climate system therefore the absence of a seasonal cycle does not affect the overall qualitative and main findings. The presence of organic, inorganic particles and dissolved molecules restrains the light penetration in the ocean (Ward et al., 2018). The vertical light attenuation scheme is given by Eq.1:

$$135 \quad I(z) = I_0 \cdot \exp(-k_w \cdot z - k_{Chl} \cdot \int_0^z Chl(z) \cdot dz) \qquad (1)$$

where $I(z)$ is the irradiation of the full solar spectrum at depth z, I_0 is the irradiation at the surface of the ocean, k_w is light absorption by clear water and inorganic particles (0.04 m^{-1}), k_{Chl} is the light absorption by chlorophyll (0.03 m^{-1}(mg Chl)$^{-1}$) and $Chl(z)$ is the chlorophyll concentration at depth z. The values for k_w and k_{Chl} are taken from Ward et al. (2018). The parameter I_0 is negative in the model because it is a downward flux from the sun to the surface of the ocean. We allow primary

140 production and light to penetrate until the sixth layer of the model (221.84 m deep), which is the lower limit of the euphotic zone (Tett, 1990). In our model setup, maximum absorption occurs in the upper oceanic layer and minimum absorption occurs in the sixth layer.

Phytoplankton changes the optical properties of the ocean (Sonntag and Hense, 2011) through phytoplankton light absorption. Therefore it can cause a radiative heating and change the oceanic temperature. We implemented phytoplankton light absorption

145 into the model following Hense (2007) and Patara et al. (2012). The scheme is give by Eq.2:

$$\frac{\partial T}{\partial t} = \frac{1}{\rho \cdot c_p} \frac{\partial I}{\partial z} \qquad (2)$$

$\partial T/\partial t$ denotes the temperature changes, c_p is the specific heat capacity of water, ρ is the ocean density, I is the solar radiation incident at depth z. Part of the light absorbed is used by phytoplankton for photosynthesis and part leads to heating of the water.

2.3 Air-sea heat exchange

We detail here the total heat flux from the ocean and sea-ice going into the atmosphere. The vertically integrated atmospheric heat equation (Eq. 3) is given by Weaver et al. (2001) and Marsh et al. (2011):

$$Q_{ta} = Q_{SW} \cdot C_A + Q_{LH} + Q_{LW} + Q_{SH} - Q_{PLW} \tag{3}$$

Q_{ta} corresponds to the total heat flux into the atmosphere, Q_{SW} is the net shortwave radiation corresponding to the solar irradiance received from the sun and reflected by the planet's albedo, C_A is a heat absorption coefficient (0.3 over the ocean (Marsh et al., 2011)), Q_{LH} is the latent heat flux corresponding to phase change of a thermodynamic system, Q_{SH} is the sensible heat flux corresponding to temperature change of a thermodynamic system, Q_{LW} is the net (upward minus downward) re-emitted longwave radiation corresponding to infrared energy coming from the planet and Q_{PLW} is the outgoing planetary longwave radiation.

The atmosphere loses heat through net longwave radiation, dominated by the outgoing longwave radiation, thus the total longwave heat flux ($Q_{LW} + Q_{PLW}$) is negative in the model. Furthermore, evaporative cooling of the ocean leads to a latent heat release in the atmosphere upon condensation and precipitation. Evaporated water vapour may be transported away from an oceanic source, to condense and precipitate elsewhere.

2.4 Air-sea CO$_2$ exchange

The atmospheric temperature depends on the atmospheric CO$_2$ concentration which is affected by the transfer of CO$_2$ between the ocean and the atmosphere. The flux of CO$_2$ across the atmosphere-ocean interface (Eq. 4) is given by Ridgwell et al. (2007):

$$F_{CO_2} = k \cdot \rho \cdot (C_w - \alpha \cdot C_a) \cdot (1 - A) \tag{4}$$

F_{CO_2} is the air-sea CO$_2$ flux, k corresponds to the gas transfer velocity, ρ is the ocean density, C_w is the concentration of dissolved gas in the surface ocean, α is the solubility coefficient calculated from Wanninkhof (1992) and depends on the sea surface temperature and salinity, C_a is the concentration of gas in the atmosphere and A is the fraction of the ocean covered by sea-ice.

Phytoplankton light absorption warms the surface of the ocean and thus reduces CO$_2$ solubility and sea-ice fraction. The flux of CO$_2$ is therefore affected via the parameters C_w, α and A. To study precisely the flux we either prescribe these parameters in the air-sea CO$_2$ exchange calculation or let them evolve freely (see below).

3 Model setup and simulations

During this study, we are primarily interested in the relative differences between our selected simulations. We focus on the relative impact of phytoplankton light absorption on different climate pathways rather than on the changes in the climate state.

We try to simulate a realistic mean climate system but the absolute value of the climate quantities are less relevant due to the limitations of such a model of intermediate complexity.

For a realistic nutrient distribution in the ocean, we performed a BIOGEM spin-up for 10,000 years. During the spin-up the atmospheric CO_2 concentration is fixed to 278 ppm. The simulations restart for 1,000 years after the spin-up with ECOGEM, meaning that all simulations consider marine biota. Due to the single layer atmospheric component, the non-seasonality and the non-representation of the land dynamics, running the model for 1,000 years is sufficient to achieve steady-state. The results represent the annual mean of the last year of the simulations, when the model is in steady-state. The present-day continental configuration, model setup, grid resolution and ecosystem community are identical as in Asselot et al. (2021). Our model setup has a reasonable match to observations and further details can be found in Asselot et al. (2021). For simplification, only one phytoplankton and one zooplankton species are included in the model setup (Appendix A1 and B1). Repeating our main simulations with multiple size classes leads in small differences compared to the simulations with one size class. Unlike our previous study, prescribing SST is necessary for some simulations here. Due to technical issues, we cannot prescribe the seasonal cycle of SST but only the annually-averaged SST. As a consequence, the seasonality is removed from our model setup. The absence of the seasonal cycle is not an issue for this study because we look at the importance of each climate pathway rather than focusing on the quantitative changes of the climate system.

The carbon cycle is closed in our simulations, meaning that there is no input of carbon through volcanic or anthropogenic activities. Only the size of the carbon reservoirs can vary. If not stated otherwise, the concentration of atmospheric CO_2 evolves freely in the simulations. All simulations are forced with the same constant flux of dissolved iron into the ocean surface (Mahowald et al., 2006). To ensure that the model is suitable for our study, we conducted two sensitivity analyses. First, we analyzed the sensitivity of the climate variables by conducting two simulations with different atmospheric CO_2 concentrations (Appendix C1). Second, we ensure that the heat and CO_2 interaction is negligible (Appendix D1). To study the effect of phytoplankton light absorption on the atmospheric temperature we perform seven different simulations, all including the ECOGEM component (Figure 3):

- *Bio* is the reference run and is the only simulation that does not include phytoplankton light absorption ($k_{Chl} = 0$ in Eq. 1). In this simulation, all the climate pathways evolve freely.

- *BioLA* is the same as the reference run but phytoplankton light absorption is implemented. In this simulation, all the climate pathways evolve freely.

- *HEAT* is the same as the second one except that we prescribe the atmospheric CO_2 concentration only for the atmospheric temperature calculation. For a comparison with the reference run, the prescribed atmospheric CO_2 concentration from *Bio* is used (169 ppm). The effect of CO_2 on atmospheric temperature is fixed but the air-sea heat fluxes evolve freely. This simulation analyses the effect of phytoplankton-induced changes of air-sea heat fluxes on the atmospheric temperature.

– *CARB* is the simulation with an uncoupled ocean-atmosphere setup. The atmospheric component is forced with the heat fluxes from *Bio* and the atmospheric CO_2 concentration is prescribed with the value of *BioLA*. This simulation determines the effect of phytoplankton-induced changes of atmospheric CO_2 concentration on the atmospheric temperature. Please note that *CARB* is well suited for studying the atmosphere properties but not to examine ocean dynamics.

– *HCorg* where we only allow the biogeochemical pumps (soft-tissue pump and carbonate pump) to affect the dissolved CO_2. The solubility of CO_2 (α in Eq. 4) and sea-ice extent (A in Eq. 4) parameters are prescribed using the respective values from *Bio*. The CO_2 solubility is fixed by prescribing the SST only for this calculation. In *HCorg* air-sea heat exchange and the biogeochemical pumps parameter (C_w in Eq. 4) evolve freely.

– *HCorgSI* where the biogeochemical pumps and sea-ice extent affect dissolved CO_2. The CO_2 solubility (α in Eq. 4) is prescribed using the value of *Bio*. In *HCorgSI* the air-sea heat exchange, the biogeochemical pumps (C_w in Eq. 4) and sea-ice extent (A in Eq. 4) parameters evolve freely.

– *HCorgSol* where the biogeochemical pumps and the solubility pump affect dissolved oceanic CO_2. The sea-ice extent parameter (A in Eq. 4) is prescribed using the value of *Bio*. In *HCorgSol* the air-sea heat exchange, the biogeochemical pumps (C_w in Eq. 4) and the CO_2 solubility (α in Eq. 4) parameters evolve freely.

4 Global response of the climate system

In this section we present the results of the simulations on a global scale. We do not consider local patterns because we removed any seasonal cycle in our model setup. Moreover, the horizontal grid resolution is low and marine biota cannot move between grid cells, thus even if seasonality was included, key regional patterns will not be resolved. First, we focus on the chlorophyll biomass and sea surface temperature because phytoplankton light absorption has a direct effect on these climate variables (Oschlies, 2004; Lengaigne et al., 2007; Paulsen et al., 2018). Second, these changes in oceanic properties affect the carbon cycle (Manizza et al., 2008; Asselot et al., 2021), therefore we study the changes in atmospheric CO_2 concentration. Third, phytoplankton light absorption alters the atmospheric properties (Patara et al., 2012), thus we analyze the changes in radiative heat fluxes, humidity and evaporation. Finally, the response of the surface atmospheric temperature is analyzed.

4.1 Chlorophyll biomass and sea surface temperature

Our results indicate differences of SST and chlorophyll biomass, depending on the climate pathways included in our model setup (Table 1). Due to the uncoupled ocean-atmosphere setup in *CARB*, ocean dynamics are not presented in this section. The reference run *Bio* has the lowest chlorophyll biomass and a low SST while the simulation *BioLA* has the highest chlorophyll biomass and SST. The increase in chlorophyll biomass is due to two different mechanisms: First, phytoplankton light absorption leads to a higher surface production, enhancing the remineralization at the surface of the ocean as shown by Asselot et al. (2021). Second, phytoplankton light absorption enhances the upward vertical velocity in the upwelling regions. As a result of these two mechanisms, the surface nutrient concentrations increase, explaining the higher chlorophyll biomass. The increase

in surface chlorophyll biomass due to phytoplankton light absorption between *BioLA* and *Bio* is 0.012 mgChl/m^3, in line with a previous estimate of 0.014 mgChl/m^3 (Asselot et al., 2021). The higher chlorophyll biomass is, however, limited by the increase in zooplankton biomass applying a top-down control. Via the effect of phytoplankton light absorption, a higher surface chlorophyll biomass leads to an increase of SST. The global difference of SST between *BioLA* and *Bio* is of 0.08°C. This value is lower than previous model estimates that show a global SST increase of 0.45-1°C due to phytoplankton light absorption (Murtugudde et al., 2002; Löptien et al., 2009; Asselot et al., 2021). This underestimation of the biologically-induced SST heating is due to the non-seasonal radiative forcing of the model, decreasing the global heat budget (Appendix E1).

In *HEAT*, the chlorophyll biomass is higher while the SST is lower compared to *Bio* (Table 1). This is rather counter-intuitive and is due to changes in oceanic circulation between these two simulations. For instance, the maximum Atlantic meridional overturning circulation (AMOC) is 8.6 Sv in *HEAT* while it is 7.6 Sv in *Bio*. In *HEAT*, the SST is lower and the sea-ice cover is slightly higher (Appendix F1) compared to *Bio*, leading to more deep water formation in polar latitudes. As a result, the AMOC is enhanced in *HEAT*. The stronger oceanic circulation in *HEAT* leads to an enhanced nutrient redistribution, thus increasing the surface nutrient concentrations. For instance, the surface PO$_4$ concentration is ∼0.21 μmol/kg in *HEAT* while it is ∼0.19 μmol/kg in *Bio*. The higher surface PO$_4$ concentration in *HEAT* explains the higher chlorophyll biomass in this simulation compared to *Bio*. The enhanced oceanic circulation in *HEAT* compared to *Bio* leads also to a stronger redistribution of heat along the water column, explaining the surface cooling and the warming of the deep ocean in *HEAT*. Our results indicate that the bottom water temperature in *HEAT* is 3.57°C while it is 3.09°C in *Bio*.

The surface chlorophyll biomass in the simulations *HCorg*, *HCorgSI* and *HCorgSol* are higher than the surface chlorophyll biomass in *Bio* due to the higher surface PO$_4$ concentrations. In *Bio* the surface PO$_4$ concentration is 0.18 μmol/kg while in the simulations *HCorg*, *HCorgSI* and *HCorgSol* the surface PO$_4$ concentrations are >0.21 μmol/kg. The higher surface PO$_4$ concentrations are due to enhanced remineralization at the ocean surface and enhanced upward vertical velocities in the upwelling regions. Due to the effect of phytoplankton light absorption, the higher surface chlorophyll biomasses in *HCorg*, *HCorgSI* and *HCorgSol* lead to higher SSTs compared to *Bio*. Only the sea-ice extent differs between the simulations *HCorg* and *HCorgSI* but their chlorophyll biomass and SSTs are identical. This result evidences a lack of sea-ice influence on these climate variables and thus on the heat fluxes. In addition, the chlorophyll biomass and SST are higher in *HCorg* compared to *HCorgSol*, indicating that the solubility factor has a negative effect on these climate variables. Between these two simulations, the only difference is the CO$_2$-solubility factor that can evolve freely in *HCorgSol*. In the simulation *HCorg*, the SST for the calculation of the CO$_2$ solubility is prescribed using the value of *Bio*, which is the lowest value. Considering the physical and chemical properties of the ocean, a low SST increases the solubility of CO$_2$ (Wanninkhof, 1992). Therefore, the CO$_2$ solubility is reduced in *HCorgSol* compared to *HCorg*, due to the higher SST in *HCorgSol*. For instance, our results indicate that on a global scale, the surface oceanic CO$_2$ concentration is 27.200 μmol/kg in *HCorgSol* while it is 27.213 μmol/kg in *HCorg*. Via the nutrient ratios, these changes in carbon cycle between the simulations affect the phosphate and iron cycles (Ward et al., 2018). As a consequence, the surface PO$_4$ concentration is ∼0.216 μmol/kg in *HCorg* and about ∼0.214 μmol/kg

275   in *HCorgSol*. The higher surface PO_4 concentration leads to a larger surface chlorophyll biomass and higher SST in *HCorg* compared to *HCorgSol*.

4.2 Atmospheric properties

The oceanic properties differ between the simulations, thus we expect differences in the atmospheric properties. We compare the atmospheric CO_2 concentration, the heat fluxes, the evaporation, the specific humidity and finally the surface atmospheric
280   temperature between the simulations.

4.2.1 Atmospheric CO_2 concentration

The atmospheric CO_2 concentrations for the simulations is low compared to the pre-industrial level (Figure 4). This is due to our new model setup that allows primary production until the sixth oceanic layer, meaning that more carbon is stored in the deep ocean, reducing the atmospheric CO_2 concentration (see Asselot et al. (2021)). In all the simulations considering
285   phytoplankton light absorption, the atmospheric CO_2 concentration is higher than in the reference run. In a previous study, we evidence that the higher atmospheric CO_2 concentration is mainly due to decrease in CO_2 solubility via the higher SST while the enhanced remineralization of organic matter and the dissolution of $CaCO_3$ slightly affect the atmospheric CO_2 concentration (Asselot et al., 2021). The atmospheric CO_2 concentration is the lowest in *Bio* while it is the highest in *BioLA*, with a difference of 9 ppm. This value is lower than a previous estimate that indicates an increase of atmospheric CO_2 concentration
290   of 18 ppm (Asselot et al., 2021). This lower estimate is due to the non-seasonal cycle forcing, neglecting the seasonal variations of air-sea CO_2 exchanges.

In *HEAT*, the atmospheric CO_2 concentration is prescribed only for the atmospheric temperature calculation. Therefore the atmospheric CO_2 concentration can vary due to changes in dissolved oceanic CO_2, sea-ice extent and CO_2 solubility, affecting
295   the other climate variables. The atmospheric CO_2 concentration in *HEAT* is slightly higher than in *Bio*. This is due to the larger chlorophyll biomass in *HEAT* than in *Bio* (Table 1), indicating a higher production and thus more remineralization in the ocean. During the remineralization process, CO_2 is produced, thus the higher remineralization in *HEAT* increases the dissolved CO_2 concentration. On a global scale, our results indicate that the surface dissolved oceanic CO_2 is about 6.354 mol/kg in *HEAT* while it is 6.302 mol/kg in *Bio*. The larger dissolved oceanic CO_2 concentration in *HEAT* increases the air-sea CO_2 flux and in
300   turn the atmospheric CO_2 concentration (see Eq. 4).

The atmospheric CO_2 concentration in *CARB* is similar to the one in *BioLA* because we prescribed the value against the one in *BioLA*.

305   The simulations *HCorg*, *HCorgSI* and *HCorgSol* have a higher atmospheric CO_2 concentration than in *Bio*. This is again not surprising because these simulations consider phytoplankton light absorption which increases the atmospheric CO_2 concentration as shown by Asselot et al. (2021). The atmospheric CO_2 concentration between *HCorg* and *HCorgSI* is similar even if their

sea-ice extent and sea-ice thickness differs (Appendix F1). The changes in sea-ice do not have an effect on the atmospheric CO_2 concentration. The slightly higher atmospheric CO_2 concentration in *HCorgSol* compared to *HCorg* is due to changes in CO_2 solubility: As described above, the CO_2 solubility is lower in *HCorgSol* compared to *HCorg*. As a consequence, the air-sea CO_2 flux is higher in *HCorgSol* compared to *HCorg*, leading to a slightly higher atmospheric CO_2 concentration in *HCorgSol*.

4.2.2 Heat fluxes

The air-sea heat flux is divided into the net shortwave radiation, the net re-emitted longwave radiation, the sensible heat flux and the latent heat flux (Figure 5). The air-sea heat fluxes represent the total heat fluxes from the ocean and sea-ice, going into the atmosphere. The simulations *HCorg* and *HCorgSI* have exactly the same heat fluxes. The only difference between these two simulations is the different sea-ice extent for the calculation of the air-sea CO_2 flux. This change in air-sea CO_2 flux does not alter the air-sea heat flux, explaining the identical radiative heat fluxes between *HCorg* and *HCorgSI*. Furthermore, the simulations *BioLA* and *HCorgSol* have the same heat fluxes and the only difference is also the sea-ice extent. As detail previously, the changes in sea-ice extent do not affect the heat fluxes, explaining the identical radiative fluxes between *BioLA* and *HCorgSol*. Finally, the heat fluxes between *CARB* and *Bio* are identical because we prescribed the heat fluxes in *CARB* with the values of *Bio*.

The net shortwave heat flux is divided in two fluxes: the incoming shortwave radiation from the sun entering the atmosphere and the outgoing reflected shortwave radiation leaving the atmosphere. Figure 5a shows that the net shortwave heat flux is identical for all the simulations and is positive. The positive values indicate that net shortwave heat flux is dominated by the flux entering the system, the incoming radiation. The incoming shortwave radiation from the sun is always identical between simulations. Therefore identical net shortwave heat flux implies that the outgoing reflected shortwave radiation is as well the same between simulations due to the treatment of shortwave radiation in the model (Weaver et al., 2001).

The net longwave heat flux is negative for all simulations, indicating that this flux is dominated by the upward longwave radiation leaving the atmosphere (Figure 5b). A more negative value of net longwave heat flux indicates a greater loss of heat to outer space. The simulations *Bio* and *CARB* have the least negative net longwave heat flux while *HEAT* has the highest negative heat flux, indicating that *HEAT* loses more heat than the others simulations. The higher heat loss in *HEAT* is due to the lowest SST and a reduced amount of greenhouse gases, precisely a low specific humidity (Figure 6) and atmospheric CO_2 concentration (Figure 4). The lower amount of greenhouse gases in the atmosphere permits a higher loss of heat outside the atmosphere. All the simulations considering phytoplankton light absorption, except *CARB* where the heat fluxes are prescribed, have a higher negative net longwave heat flux compared to *Bio*. This result is predictable because this biogeophysical mechanism is an additional heat source for the surface of the ocean, where air-sea heat exchanges occur.

The sensible heat flux depends on the atmospheric and oceanic temperature (Fanning and Weaver, 1996; Weaver et al., 2001).

The sensible heat flux increases when the atmospheric temperature decreases and when the oceanic temperature increases. For the simulation *HEAT*, the sensible heat flux is the highest (Figure 5c) because the atmospheric temperature is the lowest (Figure 7). In contrast, the sensible heat flux is the lowest for the simulation *BioLA* because the gradient of temperature between the ocean and the atmosphere is low. The sensible heat flux in *HCorg* and *HCorgSI* are close to the sensible heat flux of *Bio* because their air-sea temperature gradients are almost similar.

The global mean latent heat flux (Figure 5d) depends mainly on the global mean precipitation (Weaver et al., 2001). The simulation *Bio* has the smaller latent heat flux due to the lowest precipitation in this simulation (Appendix G1). The latent heat flux in *BioLA*, *HCorg*, *HCorgSI* and *HCorgSol* are almost similar due to their almost similar precipitations. The precipitation in *HEAT* is higher than in *Bio*, explaining the higher latent heat flux in *HEAT*.

4.2.3 Specific humidity and evaporation

The specific humidity and the evaporation in *BioLA* and *HCorgSol* are similar and the same is true between the simulations *HCorg* and *HCorgSI* (Figure 6). The specific humidity and evaporation are the lowest in *Bio* due to the lowest latent heat flux in this simulation. Including phytoplankton light absorption increases the latent heat flux and therefore increases the specific humidity and evaporation, which is consistent with Oschlies (2004) and Lengaigne et al. (2009). On a global scale, in *BioLA* the evaporation increases by 0.11%, thus enhancing the specific humidity by 0.5%. This latter value is lower than previous estimates where phytoplankton light absorption raises the specific humidity by 2-6% (Patara et al., 2012). The different values between our estimates and Patara et al. (2012) come from the non-seasonal cycle in our model setup, changing the heat budget and therefore underestimating the specific humidity. Moreover, the specific humidity in *HEAT* is lower than in *BioLA* due to the lower latent heat flux in the simulation *HEAT*. The evaporation depends on several processes and one of the most important is the humidity in the atmosphere, with lower humidity leading to higher evaporation (Weaver et al., 2001). As a consequence, the evaporation is higher in *HEAT* than in *BioLA*. Furthermore, the specific humidity and the evaporation increase when the atmospheric temperature rises (Weaver et al., 2001). The specific humidity and evaporation are higher in *CARB* compared to *BioLA* because the surface atmospheric temperature is higher in *CARB* (Figure 7). The specific humidity and evaporation in *HCorg* and *HCorgSI* are slightly lower than in *BioLA* because the latent heat flux in *HCorg* and *HCorgSI* is slightly lower. Once the CO_2 solubility factor is considered (simulation *HCorgSol*), the values of the specific humidity and evaporation are similar to the values in *BioLA*. This is not surprising because the heat fluxes between *HCorgSol* and *BioLA* are identical.

4.2.4 Surface atmospheric temperature

The difference in atmospheric properties between simulations lead to changes of the surface atmospheric temperature (Figure 7). First of all, *Bio* has a low SAT because it doesn't include the additional heat source coming from the phytoplankton light absorption mechanism. The SAT in *Bio* is 9.31°C while the SAT in *BioLA* is 9.45°C which makes a global difference of 0.14°C. This estimate is lower than previous estimates of 0.2-0.45°C (Patara et al., 2012; Asselot et al., 2021) due to the non-seasonal cycle in our model.

The lower SAT in *HEAT* compared to *Bio* is due to several reasons. Even if *HEAT* considers phytoplankton light absorption, we show that the SST in *HEAT* is lower than in *Bio*. For the SAT computation, the atmospheric CO_2 concentrations are identical between *Bio* and *HEAT*. Additionally, the specific humidity only increases by 0.27% in *HEAT* compared to *Bio*. Therefore the greenhouse gas effect between these two simulations is rather similar. However, the global net longwave heat flux decreases by $\sim$0.2 W/m^2 in *HEAT* due to the lower SST, leading to a cooling of the atmosphere. The combination of these different reasons explains the slightly lower SAT in *HEAT* compared to *Bio*.

For the simulation *CARB*, the concentration of greenhouse gases (atmospheric CO_2 and specific humidity) is higher than in *Bio* while the air-sea heat fluxes are identical. As a consequence, more heat is trapped in the atmosphere and the SAT increases by 0.71°C compared to the reference run.

The sea-ice extent is different between *HCorg* and *HCorgSI* (Appendix F1) but the response of SAT is identical, indicating that with our model setup, the changes in sea-ice extent do not affect the SAT. The specific humidity and the atmospheric CO_2 concentration are slightly higher in *HCorg* and *HCorgSI*, leading to a small increase of SAT compared to *Bio*.

In *HCorgSol* the atmospheric CO_2 concentration and the specific humidity are higher than in *Bio*. However, the sensible heat flux and the net longwave heat flux are lower in *HCorgSol*. Even if the greenhouse gases concentrations are higher, the reduced air-sea heat fluxes lead to a slight decrease in SAT in the simulation *HCorgSol* compared to *Bio*.

5   Limitations

Our study is designed to understand the climate pathways behind the phytoplankton-induced atmospheric warming but our model setup has limitations. Most notably, we do not consider a seasonal cycle in our study. Enabling seasonality would lead to larger seasonal increase of temperature but it would also lead to larger seasonal decrease in CO_2 solubility. Therefore, we suppose that the heat-pathway would not overrule the CO_2-pathway. Due to our new model setup with primary production allowed until the sixth layer of the model, the atmospheric CO_2 concentration of the simulations is lower than the pre-industrial level. Our quantitative estimates would be affected if the atmospheric CO_2 concentration of the reference run would be higher but we assume that the qualitative estimates would be very similar and the conclusions will not change. If the atmospheric CO_2 baseline is higher, also the heat budget would increase. As a consequence, the ocean would be warmer and the CO_2 solubility would decrease, increasing the importance of the CO_2 pathway in the phytoplankton-induced atmospheric warming.

This study investigates the impact of short-lived seasonal organisms, thus having an annual mean approach underestimates the effect of phytoplankton light absorption on the climate system. The absence of a nitrogen cycle could have additional effects that are not included in our study. Phytoplankton light absorption warming low-oxygen regions causes an additional

oxygen consumption, leading to hypoxia. As a consequence, we suggest that the denitrification would increase nitrogen fixation inducing a local increase in biomass. This increase in biomass would increase any pathway sensitivity of atmospheric CO_2. Moreover, several studies considering a dynamic land component and focusing on phytoplankton light absorption report an increase in heat budget due to this biogeophysical mechanism (Anderson et al., 2007; Lengaigne et al., 2009). If a land model were to be included, we speculate that we would still find an oceanic and atmospheric heating. However, the magnitude of changes might be smaller due to the uptake of CO_2 by vegetation, decreasing the atmospheric CO_2 concentration. Furthermore, the model does not include a temperature-dependency of iron bioavailability. According to previous experiments, a warming of the ocean decreases the bioavailability of iron (Liu and Millero, 2002). Phytoplankton light absorption increasing oceanic temperature might thus reduces the iron bioavailability. As a consequence, the limitation of phytoplankton growth by iron would increase, limiting the increase in chlorophyll biomass due to phytoplankton light absorption. Our study only considers two PFTs and bringing in more PFTs would be an interesting complement of our findings. For instance, observations and modeling studies indicate that positively buoyant phytoplankton groups, such as cyanobacteria, are important to study phytoplankton light absorption (Sonntag and Hense, 2011; Paulsen et al., 2018; Wurl et al., 2018). Implementing these microorganisms to assess our research question could be a beneficial follow-up of our study.

6   Conclusions

For the first time, using the EcoGEnIE model (Ward et al., 2018), we compare the role of the air-sea heat and CO_2 fluxes and quantify their influence on the biologically-induced atmospheric warming. We show that without any seasonality and with all the climate pathways included, the surface atmospheric temperature increases by $0.14°C$ due to phytoplankton light absorption. As suggested by previous studies (Capone et al., 1998; Oschlies, 2004; Wetzel et al., 2006), phytoplankton light absorption changes the air-sea heat flux. Our results indicate that when only this air-sea interaction is considered, the atmosphere cools by $0.02°C$ compared to a simulation without the biogeophysical mechanism. Moreover, when only the air-sea CO_2 exchange is considered, the atmospheric temperature increases by $0.71°C$. Clearly, our results indicate that the air-sea CO_2 exchange has a more important effect than the air-sea heat flux on the phytoplankton-induced warming of the atmosphere. With our model setup, the sea-ice extent and thickness slightly vary between simulations, therefore sea-ice processes hardly affect the air-sea CO_2 flux and thus the climate system. Moreover, including the solubility pathway changes the heat fluxes, specifically reducing the sensible heat flux and the net longwave heat flux compared to the reference simulation. As a consequence, this climate pathway has a negative effect on the atmospheric temperature. To conclude, phytoplankton light absorption influences the climate pathways at the ocean-atmosphere interface, particularly the air-sea CO_2 exchange that is important for the phytoplankton-induced atmospheric warming. For future climate studies, this work evidences that to capture the overall effect of climate-relevant mechanisms such as phytoplankton light absorption, the atmospheric CO_2 concentrations should evolve freely.

For future work, more studies with higher complexity models are necessary to make quantitative assessments rather than

qualitative assessments as in our study. Similar simulations must be conducted with a seasonal variation of the shortwave radiation to better understand the role of phytoplankton in the climate system. Moreover, a model with a dynamic atmosphere such as PLASIM-GEnIE (Holden et al., 2016) could be a good aspiration to complete our study. Indeed, previous studies evidence either an increased wind speed in subpolar regions (Patara et al., 2012) or an enhanced atmospheric dynamics (Wetzel et al., 2006; Gnanadesikan and Anderson, 2009) due to phytoplankton light absorption. The increased wind speed with a dynamic atmospheric component could thus increase the air-sea CO_2 flux, reinforcing the importance of the CO_2-pathway in our study. Finally, implementing the new temperature-dependent remineralization scheme (Crichton et al., 2021; Armstrong McKay et al., 2021) would affect the biological pump and would be an extension to our findings.

Code availability. The code for the model is hosted on GitHub and can be obtained by cloning or downloading: https://zenodo.org/record/4733736. The configuration file is named "RA.ECO.ra32lv.FeTDTL.36x36x32" and can be found in the directory "EcoGENIE_LA/genie-main/configs". The user-configuration files to run the experiments can be found in the directory "EcoGENIE_LA/genie-userconfigs/RA/Asselotetal_BG". Details of the code installation and basic model configuration can be found on a PDF file (https://www.seao2.info/cgenie/docs/muffin.pdf). Finally, section 9 of the manual provides tutorials on the ECOGEM ecosystem model.

Appendix A: Plankton functional types

We base our ecosystem community on the community described by Ward et al. (2018). However, instead of using 2 plankton functional types (PFTs) with 8 different size classes, we only use 2 PFTs with one size class (Appendix A1). We show that introducing more size classes has a smaller effect on the climate system than phytoplankton light absorption (Asselot et al., 2021). Therefore we reduced the ecosystem complexity to increase the computational time of the model.

Appendix B: Multiple size classes

We conduct two additional simulations with a higher ecosystem complexity. These simulations have 6 phytoplankton and 6 zooplankton size-classes as in Asselot et al. (2021). The simulation BioLA6 considers phytoplankton light absorption while the simulation Bio6 does not consider it. The results show that the effect of phytoplankton light absorption is reduced with a higher ecosystem complexity compared to the effect of phytoplankton light absorption with a simple ecosystem community. This is due to the higher amount of carbon stored in the living biomass with increasing number of species, thus reducing the effect of phytoplankton light absorption on the atmospheric CO_2 concentration and on the climate system.

Appendix C: Sensitivity of the climate variables

To analyze the sensitivity of the climate variables, we perform two sensitivity analyses (Appendix C1). Both simulations have the same model setup, restart from the spin-up described previously but their atmospheric CO_2 concentrations differs. The first

simulation (Sensi280) has an atmospheric CO_2 concentration of 280 ppm while the second one (Sensi320) has an atmospheric
CO_2 concentration of 320 ppm. Furthermore, the simulations Sensi280 and Sensi320 consider phytoplankton light absorption. An increase of 40 ppm in atmospheric CO_2 concentration slightly reduces the chlorophyll concentration but these changes are negligible, indicating that surface chlorophyll biomass is more sensitive to phytoplankton light absorption than an increase of 40 ppm in pCO2. The oceanic and atmospheric heat budgets are affected by the changes in atmospheric CO_2 concentration. Increasing the greenhouse gas concentrations increases in turn the SAT and therefore the SST due to the exchange of heat between the ocean and the atmosphere.

Appendix D: Air-sea fluxes interactions

To estimate the unique effect of each climate pathway we ensure that the heat and CO_2 interaction is negligible by conducting sensitivity analyses. Due to the model setup, the flux of CO_2 across the air-sea interface (F_{CO_2}; Eq. 4) depends on the SST via the Schmidt number (Wanninkhof, 1992; Ridgwell et al., 2007). We conduct two comparable sensitivity analyses and study the changes in F_{CO_2}. First, we artificially increase the SST by 1°C (Appendix D1). This increase in SST only enhances F_{CO_2} by $4.26 \cdot 10^{-5}$ mol/m^2/yr, representing a raise of 2.58% of the total air-sea CO_2 exchange. Second, the mean wind speed affects the F_{CO_2} via the gas transfer velocity (k; Eq. 4). We increase the wind speed by 0.2 m/s, which is a comparable forcing of the artificial increase of 1°C of SST. Indeed, Knutson and Tuleya (2004) indicates that a SST increase of 1°C would increase the intensity of the atmosphere dynamics and the tropical wind speed by 0.2 m/s. This increase in mean wind speed enhances the F_{CO_2} by $1.44 \cdot 10^{-4}$ mol/m^2/yr, representing an increase of 8.69% of the total air-sea CO_2 flux. Clearly, the changes in wind speed are much larger than the changes in SST hence we consider that the effect of SST on the air-sea CO_2 exchange is small enough to be neglected. Between our simulations, the maximum change of F_{CO_2} is only 0.21% which, for instance, increases the atmospheric CO_2 concentration by 0.55% and decreases the DOC by 0.71%. This small increase slightly affects the carbon reservoirs in our simulations by $< 1\%$.

Appendix E: Seasonal and non-seasonal cycle

We compare two model simulations with phytoplankton light absorption. The model setups are similar except that we switched off the seasonal cycle in one simulation. Turning off the seasonal cycle decreases the mean annual SST by 0.77°C. Furthermore, the difference of atmospheric CO_2 concentration is 6 ppm. This difference is due to different SST and therefore different CO_2 solubility between these simulations. Our results without seasonality indicate that the difference of SST between BioLA and Bio is 0.14°C. Similar simulations have been conducted with a seasonal cycle and the SST difference is 0.33°C (Asselot et al., 2021). The absence of a seasonal cycle reduces the difference of SST between the simulations with and without phytoplankton light absorption.

Appendix F: Sea-ice

The global sea-ice cover and the global sea-ice area between the simulations HCorg and HCorgSI are identical, explaining their identical climate state. Moreover, the variation of sea-ice between all simulations is small. The maximum global sea-ice cover change of 1.42% occurs between the simulations CARB and HCorgSol.

Appendix G: Precipitation

Slight fluctuations in precipitation are visible in the Appendix G1. First of all, the precipitation between *BioLA* and *HCorgSol* are similar and the same is true for the precipitation between *HCorg* and *HCorgSI*. The precipitation rate is the highest in the simulation *BioLA* due to the important specific humidity. In contrast, *HEAT* has a low specific humidity explaining the lowest precipitation rate for this simulation.

Author contributions. All authors designed and developed the concept of the study. RA performed the analysis of the model outputs with inputs from IH. RA drafted the initial version of the manuscript in collaboration with IH. All co-authors read and reviewed the final version of the manuscript.

Competing interests. The authors declare that they have no conflict of interest.

Acknowledgements. Our special thanks go to Félix Pellerin, Maike Scheffold and Laurin Steidle for their valuable comments on the early version of this manuscript. We thank David A. McKay, Alexandre Pohl and an anonymous reviewer for their helpful comments. This work was supported by the Center for Earth System Research and Sustainability (CEN), University of Hamburg, and contributes to the Cluster of Excellence "CLICCS - Climate, Climatic Change, and Society".

References

Adloff, M., Greene, S. E., Parkinson, I. J., Naafs, B. D. A., Preston, W., Ridgwell, A., Lunt, D. J., Jiménez, J. M. C., and Monteiro, F. M.: Unravelling the sources of carbon emissions at the onset of Oceanic Anoxic Event (OAE) 1a, Earth and Planetary Science Letters, 530, 115 947, 2020.

Alvarez, S. A., Gibbs, S. J., Bown, P. R., Kim, H., Sheward, R. M., and Ridgwell, A.: Diversity decoupled from ecosystem function and resilience during mass extinction recovery, Nature, 574, 242–245, 2019.

Anderson, W., Gnanadesikan, A., Hallberg, R., Dunne, J., and Samuels, B.: Impact of ocean color on the maintenance of the Pacific Cold Tongue, Geophysical Research Letters, 34, 2007.

Armstrong McKay, D. I., Cornell, S. E., Richardson, K., and Rockström, J.: Resolving ecological feedbacks on the ocean carbon sink in Earth system models, Earth System Dynamics, 12, 797–818, 2021.

Asselot, R., Lunkeit, F., Holden, P. B., and Hense, I.: The relative importance of phytoplankton light absorption and ecosystem complexity in an Earth system model, Journal of Advances in Modeling Earth Systems, 13, e2020MS002 110, 2021.

Cameron, D. R., Lenton, T. M., Ridgwell, A. J., Shepherd, J. G., Marsh, R., and Yool, A.: A factorial analysis of the marine carbon cycle and ocean circulation controls on atmospheric CO_2, Global Biogeochemical Cycles, 19, 2005.

Capone, D. G., Subramaniam, A., Montoya, J. P., Voss, M., Humborg, C., Johansen, A. M., Siefert, R. L., and Carpenter, E. J.: An extensive bloom of the N_2-fixing cyanobacterium Trichodesmium erythraeum in the central Arabian Sea, Marine Ecology Progress Series, 172, 281–292, 1998.

Claussen, M., Mysak, L., Weaver, A., Crucifix, M., Fichefet, T., Loutre, M.-F., Weber, S., Alcamo, J., Alexeev, V., Berger, A., Calov, R., Ganopolski, A., Goosse, H., Lohmann, G., Lunkeit, F., Mokhov, I., Petoukhov, V., Stone, P., and Wang, W.: Earth system models of intermediate complexity: closing the gap in the spectrum of climate system models, Climate dynamics, 18, 579–586, 2002.

Colbourn, G.: Weathering effects on the carbon cycle in an Earth System Model, Ph.D. thesis, University of East Anglia, 2011.

Crichton, K. A., Wilson, J. D., Ridgwell, A., and Pearson, P. N.: Calibration of temperature-dependent ocean microbial processes in the cGENIE. muffin (v0. 9.13) Earth system model, Geoscientific Model Development, 14, 125–149, 2021.

Edwards, N. R. and Marsh, R.: Uncertainties due to transport-parameter sensitivity in an efficient 3-D ocean-climate model, Climate Dynamics, 24, 415–433, 2005.

Fanning, A. F. and Weaver, A. J.: An atmospheric energy-moisture balance model: Climatology, interpentadal climate change, and coupling to an ocean general circulation model, Journal of Geophysical Research: Atmospheres, 101, 15 111–15 128, 1996.

Gnanadesikan, A. and Anderson, W. G.: Ocean water clarity and the ocean general circulation in a coupled climate model, Journal of Physical Oceanography, 39, 314–332, 2009.

Greene, S., Ridgwell, A., Kirtland Turner, S., Schmidt, D. N., Pälike, H., Thomas, E., Greene, L., and Hoogakker, B.: Early Cenozoic decoupling of climate and carbonate compensation depth trends, Paleoceanography and paleoclimatology, 34, 930–945, 2019.

Hense, I.: Regulative feedback mechanisms in cyanobacteria-driven systems: a model study, Marine Ecology Progress Series, 339, 41–47, 2007.

Holden, P. B., Edwards, N. R., Fraedrich, K., Kirk, E., Lunkeit, F., and Zhu, X.: PLASIM–GENIE v1. 0: a new intermediate complexity AOGCM, Geoscientific Model Development, 9, 3347–3361, 2016.

Kahru, M., Leppanen, J.-M., and Rud, O.: Cyanobacterial blooms cause heating of the sea surface, Marine Ecology Progress Series, 101, 1–7, 1993.

Knutson, T. R. and Tuleya, R. E.: Impact of CO_2-induced warming on simulated hurricane intensity and precipitation: Sensitivity to the choice of climate model and convective parameterization, Journal of climate, 17, 3477–3495, 2004.

Kowalczuk, P., Sagan, S., Makarewicz, A., Meler, J., Borzycka, K., Zabłocka, M., Zdun, A., Konik, M., Darecki, M., Granskog, M. A., et al.: Bio-optical properties of surface waters in the Atlantic water inflow region off Spitsbergen (Arctic Ocean), Journal of Geophysical Research: Oceans, 124, 1964–1987, 2019.

Lengaigne, M., Menkes, C., Aumont, O., Gorgues, T., Bopp, L., André, J.-M., and Madec, G.: Influence of the oceanic biology on the tropical Pacific climate in a coupled general circulation model, Climate Dynamics, 28, 503–516, 2007.

Lengaigne, M., Madec, G., Bopp, L., Menkes, C., Aumont, O., and Cadule, P.: Bio-physical feedbacks in the Arctic Ocean using an Earth system model, Geophysical Research Letters, 36, 2009.

Lenton, T., Williamson, M., Edwards, N., Marsh, R., Price, A., Ridgwell, A., Shepherd, J., Cox, S., et al.: Millennial timescale carbon cycle and climate change in an efficient Earth system model, Climate Dynamics, 26, 687, 2006.

Lenton, T., Marsh, R., Price, A., Lunt, D., Aksenov, Y., Annan, J., Cooper-Chadwick, T., Cox, S., Edwards, N., Goswami, S., et al.: Effects of atmospheric dynamics and ocean resolution on bi-stability of the thermohaline circulation examined using the Grid ENabled Integrated Earth system modelling (GENIE) framework, Climate Dynamics, 29, 591–613, 2007.

Liu, X. and Millero, F. J.: The solubility of iron in seawater, Marine Chemistry, 77, 43–54, 2002.

Löptien, U., Eden, C., Timmermann, A., and Dietze, H.: Effects of biologically induced differential heating in an eddy-permitting coupled ocean-ecosystem model, Journal of Geophysical Research: Oceans, 114, 2009.

Mahowald, N. M., Yoshioka, M., Collins, W. D., Conley, A. J., Fillmore, D. W., and Coleman, D. B.: Climate response and radiative forcing from mineral aerosols during the last glacial maximum, pre-industrial, current and doubled-carbon dioxide climates, Geophysical Research Letters, 33, 2006.

Manizza, M., Le Quéré, C., Watson, A. J., and Buitenhuis, E. T.: Ocean biogeochemical response to phytoplankton-light feedback in a global model, Journal of Geophysical Research: Oceans, 113, 2008.

Marsh, R., Müller, S., Yool, A., and Edwards, N.: Incorporation of the C-GOLDSTEIN efficient climate model into the GENIE framework: "eb_go_gs" configurations of GENIE, Geoscientific Model Development, 4, 957–992, 2011.

Meyer, K., Ridgwell, A., and Payne, J.: The influence of the biological pump on ocean chemistry: implications for long-term trends in marine redox chemistry, the global carbon cycle, and marine animal ecosystems, Geobiology, 14, 207–219, 2016.

Murtugudde, R., Beauchamp, J., McClain, C. R., Lewis, M., and Busalacchi, A. J.: Effects of penetrative radiation on the upper tropical ocean circulation, Journal of Climate, 15, 470–486, 2002.

Ödalen, M., Nycander, J., Oliver, K. I., Brodeau, L., and Ridgwell, A.: The influence of the ocean circulation state on ocean carbon storage and CO_2 drawdown potential in an Earth system model, Biogeosciences, 15, 1367–1393, 2018.

Oschlies, A.: Feedbacks of biotically induced radiative heating on upper-ocean heat budget, circulation, and biological production in a coupled ecosystem-circulation model, Journal of Geophysical Research: Oceans, 109, 2004.

Patara, L., Vichi, M., Masina, S., Fogli, P. G., and Manzini, E.: Global response to solar radiation absorbed by phytoplankton in a coupled climate model, Climate dynamics, 39, 1951–1968, 2012.

Paulsen, H., Ilyina, T., Jungclaus, J. H., Six, K. D., and Stemmler, I.: Light absorption by marine cyanobacteria affects tropical climate mean state and variability, Earth System Dynamics, 9, 1283–1300, 2018.

Reinhard, C. T., Planavsky, N. J., Ward, B. A., Love, G. D., Le Hir, G., and Ridgwell, A.: The impact of marine nutrient abundance on early eukaryotic ecosystems, Geobiology, 18, 139–151, 2020.

590 Ridgwell, A., Hargreaves, J., Edwards, N. R., Annan, J., Lenton, T. M., Marsh, R., Yool, A., and Watson, A.: Marine geochemical data assimilation in an efficient Earth system Model of global biogeochemical cycling, Biogeosciences, 4, 87–104, 2007.

Sathyendranath, S., Gouveia, A. D., Shetye, S. R., Ravindran, P., and Platt, T.: Biological control of surface temperature in the Arabian Sea, Nature, 349, 54, 1991.

Shell, K., Frouin, R., Nakamoto, S., and Somerville, R.: Atmospheric response to solar radiation absorbed by phytoplankton, Journal of
595   Geophysical Research: Atmospheres, 108, 2003.

Sonntag, S. and Hense, I.: Phytoplankton behavior affects ocean mixed layer dynamics through biological-physical feedback mechanisms, Geophysical Research Letters, 38, 2011.

Tett, P.: The photic zone, Light and Life in the Sea, pp. 59–87, 1990.

Wanninkhof, R.: Relationship between wind speed and gas exchange over the ocean, Journal of Geophysical Research: Oceans, 97, 7373–
600   7382, 1992.

Ward, B. A., Wilson, J. D., Death, R., Monteiro, F. M., Yool, A., and Ridgwell, A.: EcoGEnIE 1.0: plankton ecology in the cGEnIE Earth system model, Geoscientific Model Development, 11, 4241–4267, 2018.

Weaver, A. J., Eby, M., Wiebe, E. C., Bitz, C. M., Duffy, P. B., Ewen, T. L., Fanning, A. F., Holland, M. M., MacFadyen, A., Matthews, H. D., et al.: The UVic Earth System Climate Model: Model description, climatology, and applications to past, present and future climates,
605   Atmosphere-Ocean, 39, 361–428, 2001.

Wetzel, P., Maier-Reimer, E., Botzet, M., Jungclaus, J., Keenlyside, N., and Latif, M.: Effects of ocean biology on the penetrative radiation in a coupled climate model, Journal of Climate, 19, 3973–3987, 2006.

Wilson, J., Monteiro, F., Schmidt, D., Ward, B., and Ridgwell, A.: Linking marine plankton ecosystems and climate: a new modeling approach to the warm early Eocene climate, Paleoceanography and Paleoclimatology, 33, 1439–1452, 2018.

610 Wurl, O., Bird, K., Cunliffe, M., Landing, W. M., Miller, U., Mustaffa, N. I. H., Ribas-Ribas, M., Witte, C., and Zappa, C. J.: Warming and inhibition of salinization at the ocean's surface by cyanobacteria, Geophysical research letters, 45, 4230–4237, 2018.
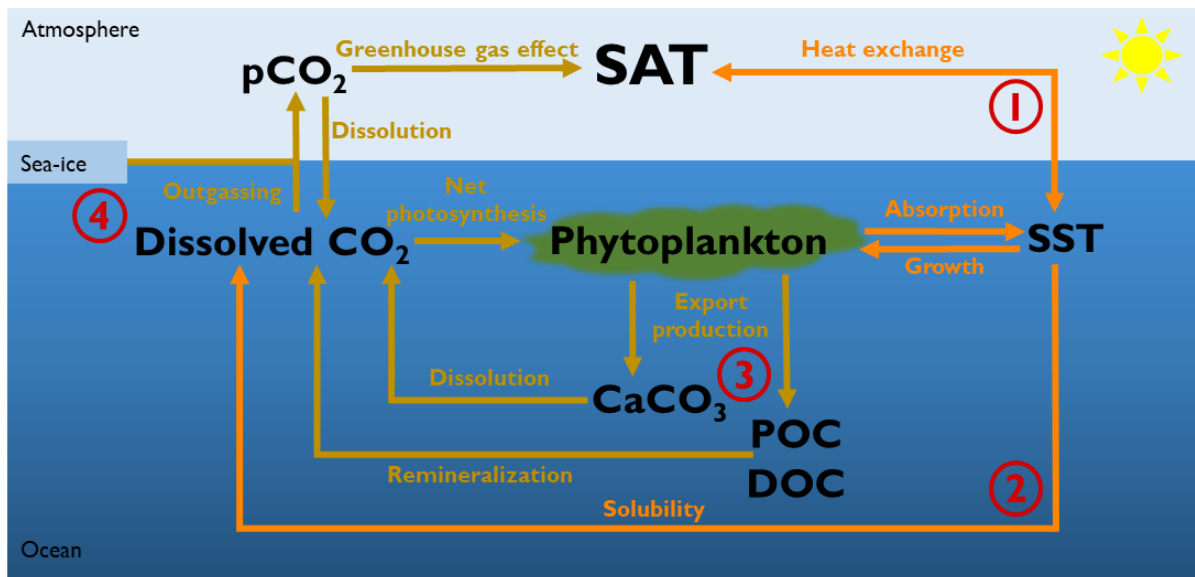
Figure 1. Representation of the four different biologically-induced pathways that affect the atmospheric temperature. (1) Marine biota via phytoplankton light absorption increases the SST, changing therefore the air-sea heat exchange and the atmospheric temperature. (2) Changes in SST also alter the solubility of CO_2 and its dissolved concentration. In turn, changes in dissolved CO_2 concentrations alter the air-sea CO_2 exchange and thus the greenhouse gas effect. (3) Phytoplankton light absorption modifies the marine biogeochemical cycles and particularly the export production of carbon. These changes in export production of carbon modify the dissolved CO_2 concentration and the greenhouse gas effect. (4) A warmer surface of the ocean can decrease the sea-ice extent. A reduction of sea-ice cover increases the air-sea CO_2 exchange area, changing the greenhouse gas concentrations. SAT = surface atmospheric temperature. SST = sea surface temperature. $CaCO_3$ = calcium carbonate. POC = particulate organic carbon. DOC = dissolved organic carbon.
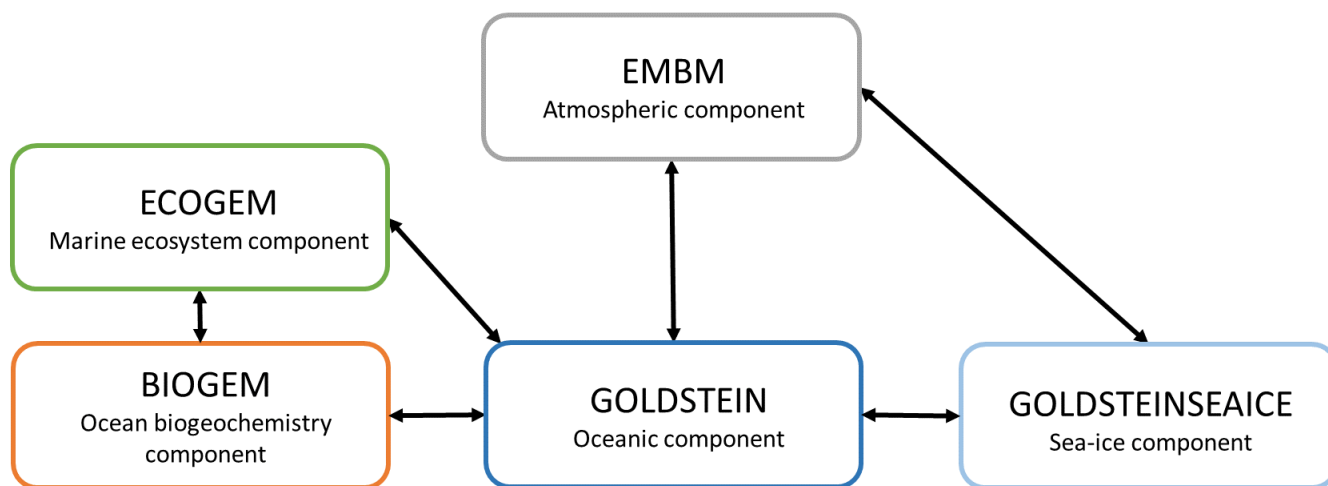
Figure 2. Representation of the components of the EcoGEnIE model. The black arrows indicate the link between the different climatic components.
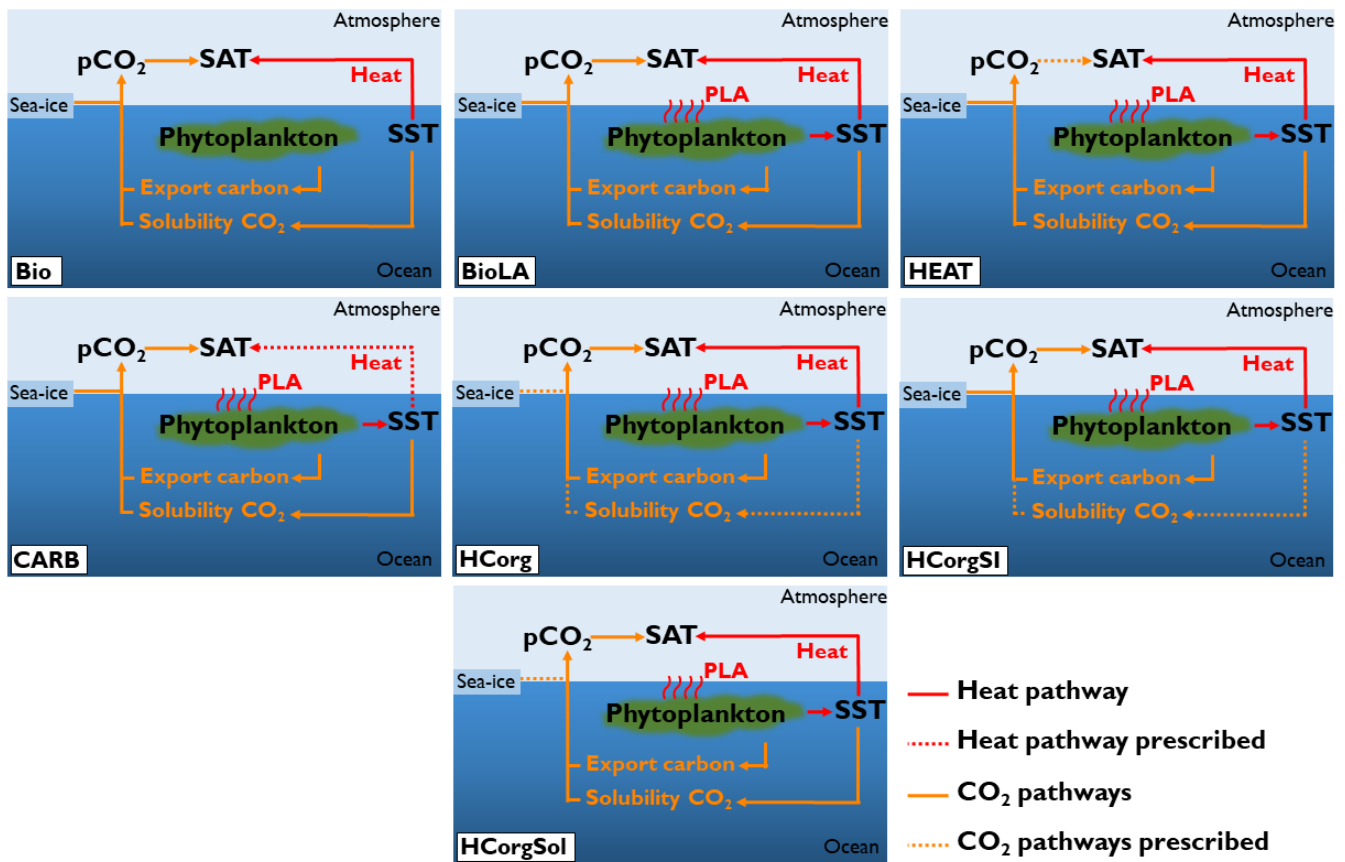
Figure 3. Sketch representing the climate pathways involved in the seven simulations (PLA = Phytoplankton Light Absorption). Note that this figure is a simplification of Figure 1, only the relevant pathways are represented. The name of the simulations are on the bottom left of each panel. The dashed arrows indicate the climate pathways prescribed. All the prescribed pathways are from the reference simulation *Bio* except the pathway between atmospheric CO_2 and SAT in *CARB* which is prescribed from the simulation *BioLA*.
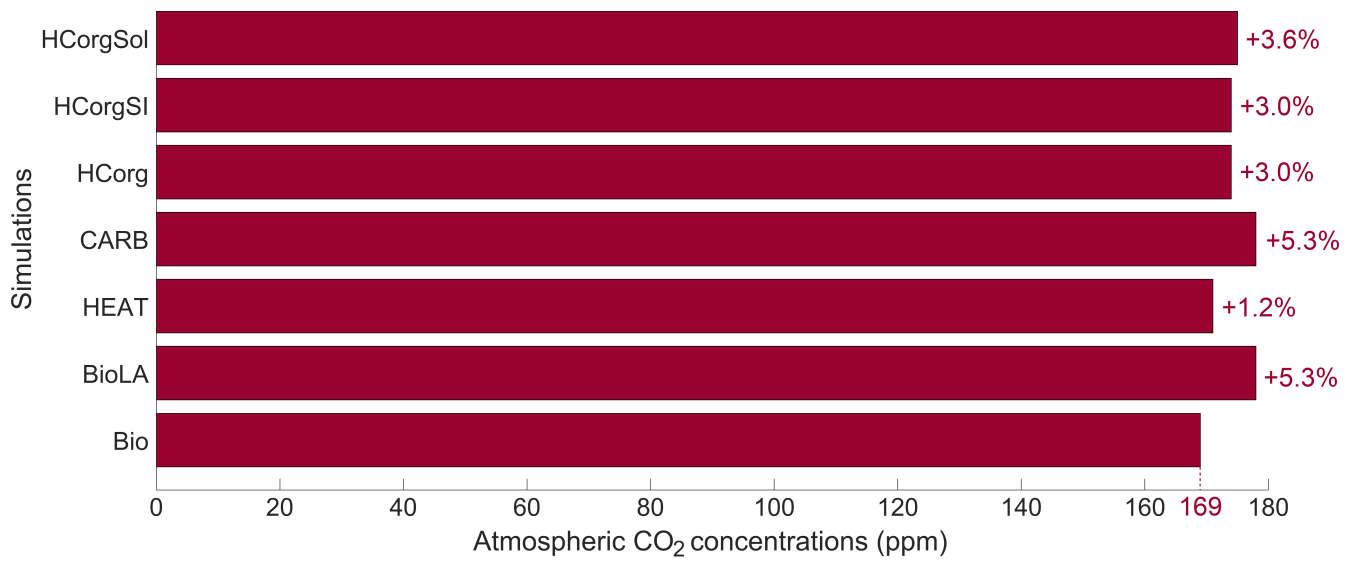
Figure 4. Atmospheric CO$_2$ concentrations (ppm) for the different simulations. The percentages represent the relative changes compared to the reference simulation Bio.
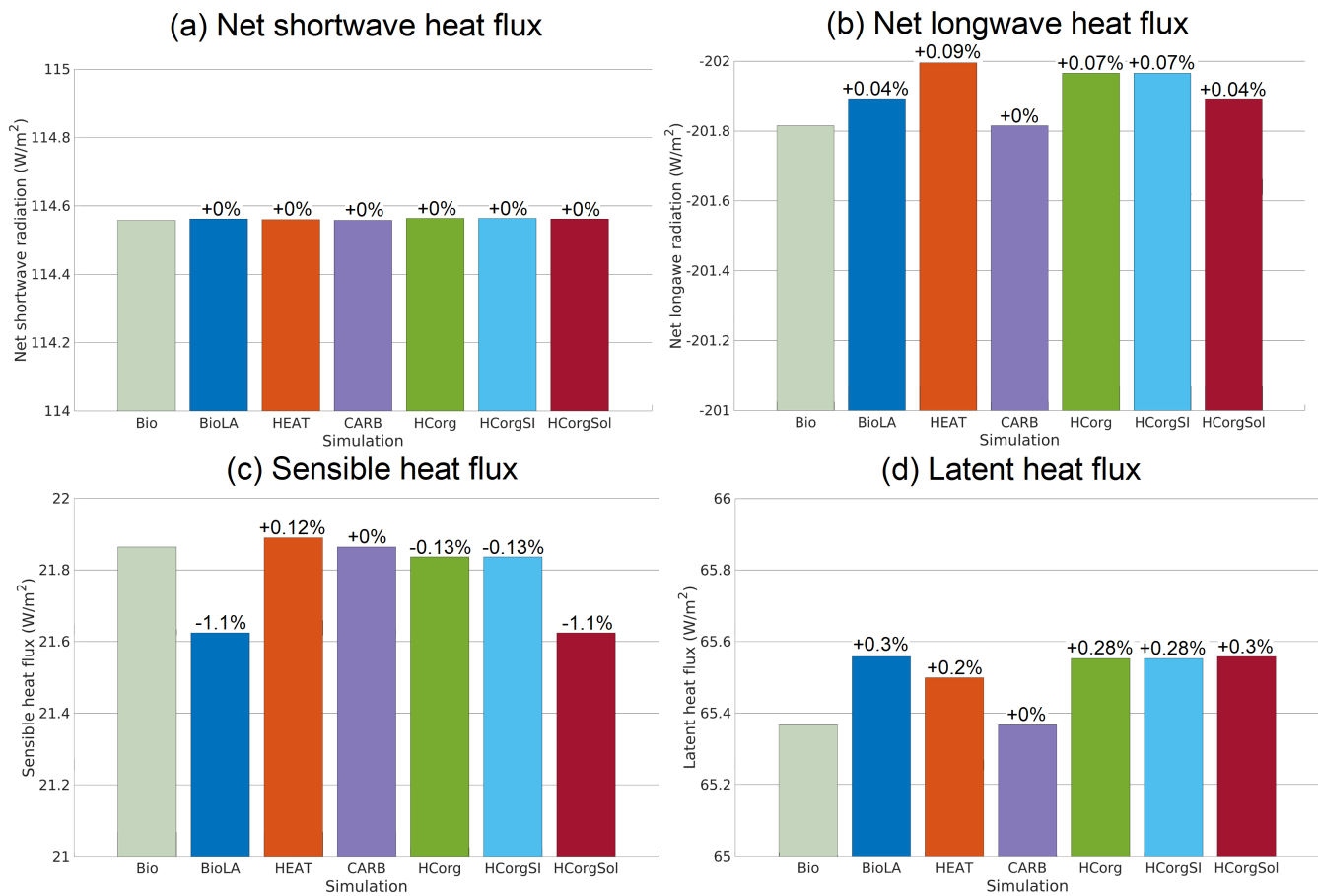
Figure 5. Global average of the different air-sea heat fluxes (W/m^2) for the seven simulations. (a) Net shortwave radiation at the top of the atmosphere. (b) Net re-emitted longwave radiation. The net longwave radiation is negative because it is dominated by the outgoing longwave radiation. (c) Sensible heat flux. (d) Latent heat flux. The color coding between the panels remains the same. The percentages represent the relative changes compared to *Bio*.
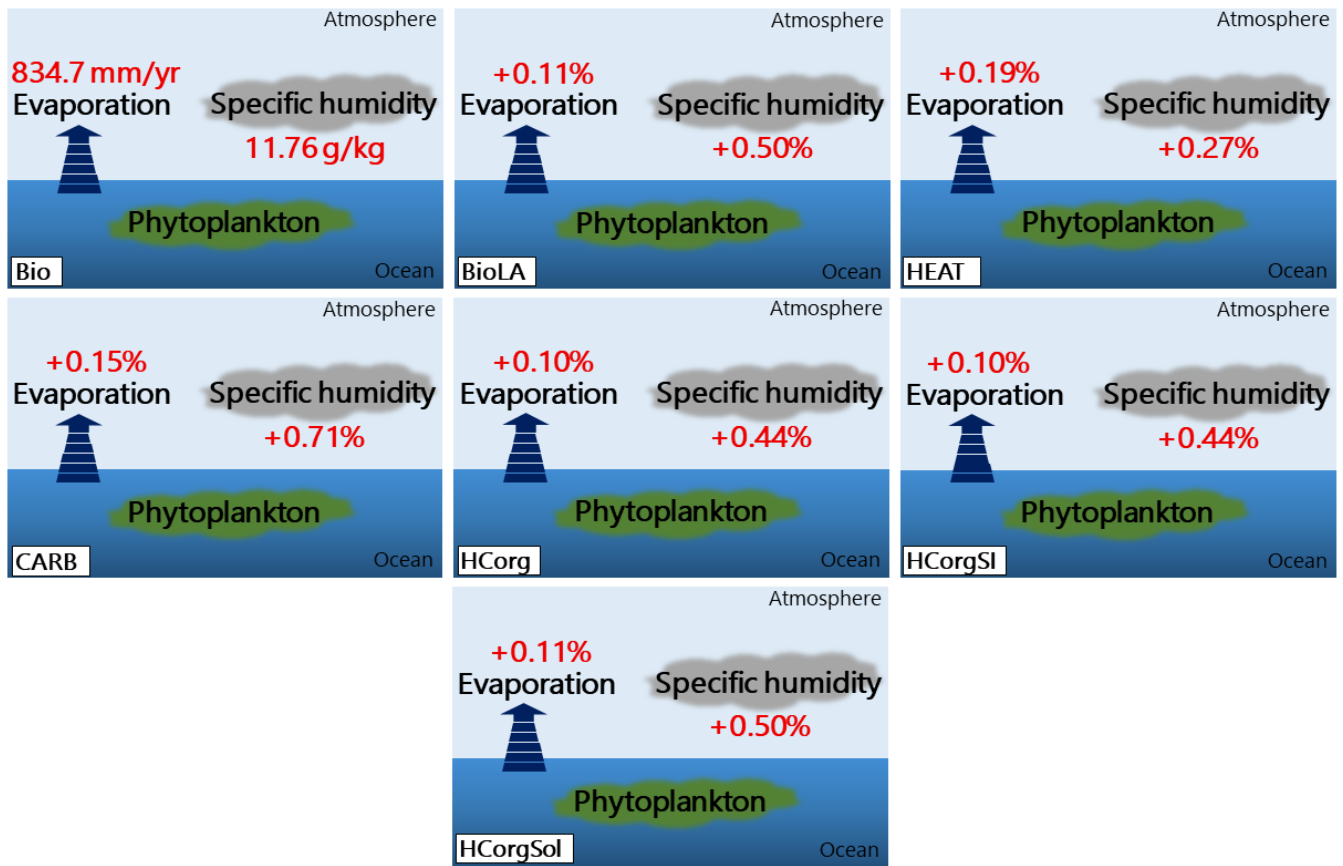
Figure 6. Evaporation (mm/yr) and specific humidity (g/kg) for the seven simulations. The percentages represent the relative changes compared to *Bio*. The name of the simulations are on the bottom left of each panel.
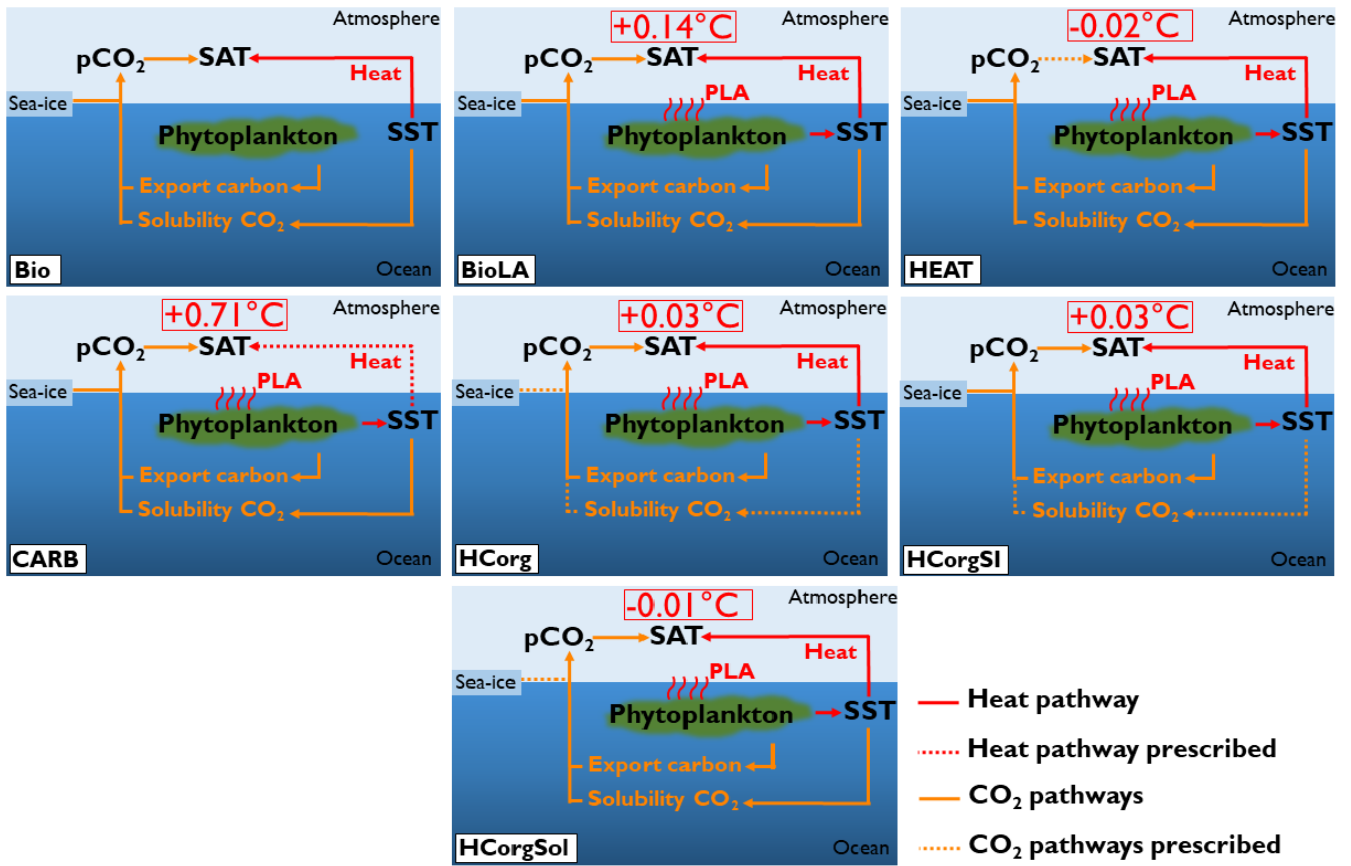
Figure 7. Sketch representing the surface atmospheric temperature (SAT) changes between the simulations and the reference run. On top is located the value of SAT change compared to *Bio*. The rest of the sketch is similar to Figure 3.

Table 1. Sea surface temperature (°C) and surface chlorophyll biomass (mgChl/m^3). There is no value for the simulation CARB because we run the model with an uncoupled ocean-atmosphere setup.

Simulation	SST (°C)	Chlorophyll biomass (mgChl/m^3)
Bio	15.26	0.09949
BioLA	15.34	0.11178
HEAT	15.25	0.10827
CARB	-	-
HCorg	15.30	0.10964
HCorgSI	15.30	0.10964
HCorgSol	15.28	0.10891

Table A1. Size of the different plankton functional types (μm) used during the simulations.

PFT	Size (μm)
Phytoplankton	46.25
Zooplankton	146.15

Table B1. Values of the most important climate quantities for the simulations with 6 phyto- and 6 zooplankton size-classes. The third row represents the differences between the simulation with minus without phytoplankton light absorption.

Simulation	Atm. CO_2 (ppm)	Chl. (mgChl/m^3)	SST (°C)	SAT (°C)
Bio6	154	0.133	14.99	8.93
BioLA6	159	0.140	15.04	8.97
Difference	+5	+0.007	+0.05	+0.04

Table C1. Chlorophyll concentration (mgChl/m^3), sea and atmospheric surface temperature (°C) for the sensitivity analysis of the climate. The difference represents the value of Sensi320 minus the value of Sensi280.

Simulation	Chloro. conc. (mgChl/m^3)	SST (°C)	SAT (°C)
Sensi280	0.1177	16.78	11.92
Sensi320	0.1175	17.17	12.44
Difference	-0.0002	0.39	0.52

Table D1. Changes in air-sea CO_2 exchange (mol/m^2/yr and %) regarding the sensitivity of the system towards the interplay between CO_2 and heat. For the first sensitivity analysis, the SST is increased by 1°C while for the second analysis, the annual mean wind speed is raised by 0.2 m/s. The third row corresponds to the maximum difference of SST between the simulations.

Sensitivity analysis	F_{CO_2} (mol/m^2/yr)	Changes (%)
+1°C	$+4.26 \cdot 10^{-5}$	2.58
+0.2 m/s	$+1.44 \cdot 10^{-4}$	8.69
+0.08°C	$+3.40 \cdot 10^{-6}$	0.21

Table E1. Sea surface temperature (°C) and atmospheric CO_2 concentration (ppm) for simulations with and without a seasonal cycle.

Simulation	SST (°C)	Atm. CO_2 conc. (ppm)
Seasonal cycle	16.11	184
Non-seasonal cycle	15.34	178

Table F1. Global sea-ice cover (%) and global sea-ice area (km^2) for the different simulations.

Simulation	Sea-ice cover (%)	Sea-ice area (km^2)
Bio	9.79	$3.60 \cdot 10^7$
BioLA	9.76	$3.59 \cdot 10^7$
HEAT	9.91	$3.64 \cdot 10^7$
CARB	8.60	$3.16 \cdot 10^7$
HCorg	9.79	$3.60 \cdot 10^7$
HCorgSI	9.92	$3.65 \cdot 10^7$
HCorgSol	10.02	$3.68 \cdot 10^7$

Table G1. Precipitation (mm/yr) for the different simulations.

Simulation	Precipitation (mm/yr)
Bio	834.62
BioLA	837.07
HEAT	836.30
CARB	834.05
HCorg	837.00
HCorgSI	837.00
HCorgSol	837.07